Coarsening Dynamics of Dewetting Films

K. B. Glasner* and T. P. Witelski†
Department of Mathematics and Center for Nonlinear and Complex Systems, Duke University, Durham, NC 27708-0320
(Dated: May 6, 2002)

Many thin fluid films are subject to instabilities caused by a competition of short and long range intermolecular forces. After breaking into droplets connected by an ultra-thin film, the fluid will undergo a coarsening process in which droplets both move and exchange mass on slow timescales. In the context of a one-dimensional lubrication model, the slow dynamics can be characterized in terms of a finite dimensional set of evolution equations. From this, a scaling law which governs the coarsening rate is derived.

PACS numbers: 68.15.+e, 68.55.-a, 47.20.Ma

I. INTRODUCTION

The competition of attractive van der Waals forces and short range repulsive forces, like Born repulsion, can produce complex instabilities in layers of thin liquid films on solid substrates. Experimental studies have shown this behavior for polymer films [14, 28, 33, 34, 44], liquid crystal films [12, 37, 38], liquid metals [3, 12] and evaporating films [8, 21]. During these dewetting processes, droplets are formed which are connected by ultra-thin films. In analogy to spinodal decomposition described by the Cahn-Hilliard equation [6], this evolution is sometimes called spinodal dewetting [19–21].

Recent theoretical work on dewetting films has focused on the details of instability and pattern formation in early stages of the dewetting process. This process, which starts with near-rupture of the fluid layer, eventually produces an array of holes or "dry spots" in the film which become wider over time [10]. It has been suggested that the propagation of the initial instability of a flat film may be controlled by either linear or nonlinear mechanisms [1, 30, 31, 35, 36, 45]. Eventually rims of the growing holes merge, giving rise to polygonal-shaped networks of fluid ridges [28, 32]. These ridges are themselves unstable, and eventually break into isolated droplets, whose structure has been studied [2, 18]. In this article, we explore the long-time dynamics, in which isolated droplets formed in the initial stages of dewetting slowly move and exchange mass to "coarsen" and yield fewer, larger droplets.

In the limit of low Reynolds number and large aspect ratio, lubrication theory [22] may be used to describe the evolution of a film of thickness $h = h(x, y, t)$. Models incorporating intermolecular forces between the fluid and the substrate which exhibit dewetting processes have been used for many years [7, 22]. More recently these models have been re-derived using a variational, diffuse interface approach [25, 26]. In non-dimensional form, the model is a degenerate, fourth-order parabolic diffusion equation

$$\frac{\partial h}{\partial t} = \nabla \cdot (h^3 \nabla p), \tag{1.1}$$

where the pressure p in the thin film is given by

$$p = \Pi(h) - \nabla^2 h. \tag{1.2}$$

The combined effects of all intermolecular forces, such as van der Waals interactions and Born repulsion, for a homogeneous film of thickness h on a solid substrate is given by the disjoining pressure, the derivative of the potential $U(h)$,

$$\Pi(h) \equiv \frac{dU}{dh}. \tag{1.3}$$

The Laplacian term in (1.2) gives the linearized contribution of surface tension to the total pressure for a slowly-varying curved interface.

---

*Electronic address: `glasner@math.duke.edu`
†Electronic address: `witelski@math.duke.edu`

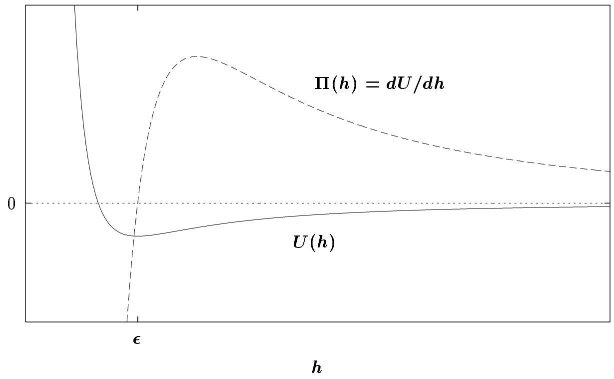

FIG. 1: Sketch of the intermolecular potential $U(h)$ and the disjoining pressure $\Pi(h) = dU/dh$.

Our analysis will describe the dynamics of coarsening for a broad class of dewetting films described by an intermolecular potential satisfying a few basic assumptions. We only need to assume the following in the structure of the potential $U(h)$:

$$U(h) \text{ has a unique minimum at } h = \epsilon \tag{1.4}$$
$$\Pi(h) \text{ has a unique maximum } p_{\max} \text{ at } h_{\text{peak}} > \epsilon \tag{1.5}$$
$$\Pi(h) = o(h^{-1}) \text{ and } U(h) \to 0 \text{ as } h \to \infty \tag{1.6}$$
$$\lim_{h\to 0} U(h) = \infty \tag{1.7}$$

Figure 1 shows a typical plot of the potential $U(h)$ and the corresponding pressure $\Pi(h)$. Property (1.4) defines the film thickness $h = \epsilon$ corresponding to the globally stable homogeneous film. This film thickness establishes the scale of the ultra-thin film (UTF) which will connect metastable liquid droplets resulting after the destabilization of the initial fluid layer. Property (1.5) states that there is a film thickness for which conjoining and disjoining pressures balance; this is necessary for there to exist stable localized droplet solutions [2]. Property (1.6) requires that the disjoining pressure is negligible for thick films, $h \gg \epsilon$. Finally, (1.7) states that the short-range repulsive intermolecular forces are assumed to be dominant at very short scales. Early studies of van der Waals driven instabilities of thin films by Williams and Davis [4, 41] and de Gennes [7] did not include these effects, and in this case classical solutions of equation (1.1) can cease to exist in finite time due to singularities which occur if the film ruptures, $h \to 0$ [42, 46]. In contrast, with (1.7) the problem is globally well-posed [2] and solutions exist for all times.

One focus of this paper is to consider limit of small ϵ while simultaneously keeping the interaction energies finite. To this end, we will suppose that the potential can be written in the form

$$U(h) = \mathcal{U}(h/\epsilon), \tag{1.8}$$

where $\mathcal{U}$ is independent of ϵ. Property (1.4) implies that the function $\mathcal{U}$ has a unique minimum at 1, and property (1.6) states that the disjoining pressure satisfies $\Pi(h) = \epsilon^{-1}\mathcal{U}'(h/\epsilon) = o(\epsilon/h)$ as $h \to \infty$. A potential which satisfies all of the above assumptions is given by $\mathcal{U}(\theta) = \theta^{1-m}/(m-1) - \theta^{1-n}/(n-1)$ with $1 < n < m$, which yields the effective conjoining/disjoining pressure

$$\Pi(h) = \epsilon^{-1}\left(\frac{\epsilon}{h}\right)^n \left[1 - \left(\frac{\epsilon}{h}\right)^{m-n}\right]. \tag{1.9}$$

For this model, the maximum pressure, $p_{\max} = O(\epsilon^{-1})$, is achieved at $h_{\text{peak}} = (m/n)^{1/[m-n]}\epsilon$, and the absolute minimum pressure for $h \geq \epsilon$ is $\Pi(\epsilon) = 0$. This particular potential was considered in [2], and with the exponents $(n, m) = (3, 9)$ it corresponds to the standard 6-12 Lennard-Jones potential [13, 19, 20, 22].

The one-dimensional dynamical equations then reads

$$\frac{\partial h}{\partial t} = \frac{\partial}{\partial x}\left(h^3 \frac{\partial}{\partial x}\left[\Pi(h) - \frac{\partial^2 h}{\partial x^2}\right]\right). \tag{1.10}$$

In working with this problem, it is convenient to study the solution in terms of the associated pressure

$$p \equiv \Pi(h) - h_{xx} = \epsilon^{-1}\mathcal{U}'(h/\epsilon) - h_{xx}, \tag{1.11}$$

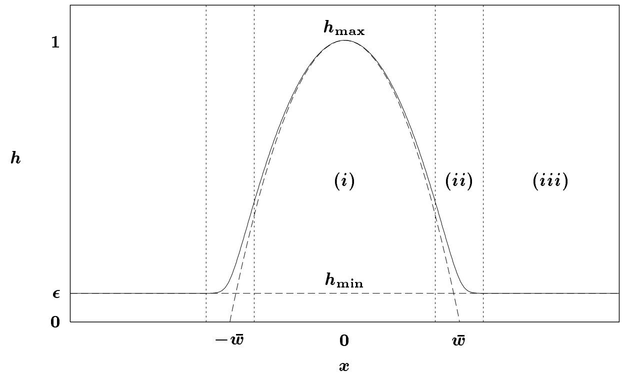

FIG. 2: A stable steady-state droplet solution $\bar{h}(x;\bar{p})$ showing the three regions in the asymptotic structure of the solution for $\epsilon \to 0$: (i) droplet core, (ii) contact line, (iii) outer ultra-thin film. The dashed curve shows the leading order asymptotic solution for the droplet core, the parabola (2.7), with width $2\bar{w}$.

and the flux

$$J \equiv -h^3 p_x. \tag{1.12}$$

Numerical simulations of thin films with generalized intermolecular forces show complex pattern formation during which films evolve to a meta-stable state composed of a collection of droplets connected by the UTF layer of thickness approximately ϵ, see Figure 4. A comparison with physical experiments shows striking similarities to the characteristic features of dewetting including the formation of capillarity ridges at the edges of growing holes (cf. [11]) as well as the development of polygonal ridge structures [27].

There is considerable similarity between our equation and the Cahn-Hilliard equation [6] whose late time behavior represents the coarsening of regions of phase separation in binary alloys. The important differences are:

- Our potential has only a single minimum, whereas Cahn-Hilliard dynamics usually considers a potential with two minima.
- The mobility coefficient in (1.10), h^3, is nearly degenerate for $h \to \epsilon$, which leads to different relaxation timescales for the droplet regions (where $h = O(1)$) and for the UTF regions (where $h = O(\epsilon)$). The original statement of the Cahn-Hilliard equation [6] included non-constant mobilities, and these have been the subject of recent studies [5].

The limiting behavior Cahn-Hilliard type equations are frequently expressed as free boundary problem problems, such as that which was formally derived by Pego [24]. In the context of a distinguished asymptotic limit, our equation will also yield a similar sort of finite-dimensional (ODE) approximation.

A further asymptotic regime of Cahn-Hilliard dynamics is described by the theories of Lifshitz and Slyozov [15] and Wagner [39], who characterize the statistical evolution of the phase separated regions (this is known popularly as "LSW theory"). Mitlin [16, 17] has proposed and studied a LSW-type model of coarsening behavior in fluid dewetting. We also study the statistics of dewetting using our finite-dimensional approximation.

In the next section, we begin with an analysis of the form of the structure of the equilibrium droplet solutions. In section III, energetic arguments are used to describe the expected long-time dynamics. In section IV, evolution equations are derived for a single near-equilibrium droplet in response to externally imposed fluxes. These evolution equations are then extended to describe the dynamics of arrays of interacting droplets in section V. And finally, in section VI a scaling law is derived to describe coarsening in very large sets of droplets.

II. STEADY STATE SOLUTIONS

Stable steady solutions of (1.10) which represent isolated fluid droplets were analyzed previously [2], and we briefly review them here. Nontrivial steady-state solutions of (1.10) have uniform, constant pressure, $p = \bar{p} \geq 0$, and consequently $h = \bar{h}(x;\bar{p})$ satisfies the second-order ordinary differential equation

$$\frac{d^2\bar{h}}{dx^2} = \Pi(\bar{h}) - \bar{p}. \tag{2.1}$$

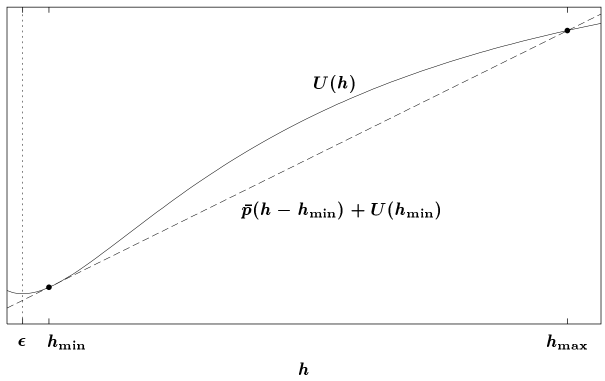

FIG. 3: Construction of $h_{\min}$ and $h_{\max}$ from the potential $U(h)$ for a droplet solution with a given value of the pressure $\bar{p}$.

Given the structure of $\Pi(h)$ for any value of $\bar{p}$ in the range $0 < \bar{p} < p_{\max}$, a phase plane analysis shows that an isolated droplet on an unbounded domain is given by the homoclinic solution of (2.1), see Figure 2. Since the maximum pressure, $p_{\max} = \Pi(h_{\text{peak}}) = O(\epsilon^{-1})$, is large, there is a continuous family of droplet solutions parametrized by the pressure $\bar{p}$. For any fixed, finite pressure in this range, $\bar{p} = O(1)$, the minimum thickness of film in the droplet solution is the $O(\epsilon)$ fixed point of (2.1), the root of the equation

$$\Pi(h_{\min}) = \bar{p}; \tag{2.2}$$

this value determines the thickness of the ultra-thin film far away from the droplet. Once $h_{\min}(\bar{p})$ is determined, we can write the first integral of (2.1) as

$$\tfrac{1}{2}\left(\frac{d\bar{h}}{dx}\right)^2 = R(\bar{h}), \tag{2.3}$$

where

$$R(\bar{h}) \equiv U(\bar{h}) - U(h_{\min}) - \bar{p}(\bar{h} - h_{\min}). \tag{2.4}$$

At the maximum of the droplet $\bar{h}_x = 0$ at $x = 0$, and hence $h_{\max}$ is determined by the condition

$$R(h_{\max}) = 0. \tag{2.5}$$

The values of $h_{\min}$, $h_{\max}$ may be given graphically by constructing the tangent-secant line for the potential $U(h)$ with slope $\bar{p}$, see Figure 3. The homoclinic solution can then be obtained from (2.3) via quadrature.

To get more insight into the droplet solutions, we consider their asymptotic properties for the limit $\epsilon \to 0$. For the limit $\epsilon \to 0$, the structure of the solution breaks down into three regimes [2] (see Figure 2): (i) *the droplet core* containing the bulk of the fluid mass, (ii) *the contact line* where asymptotic matching between the core and the outer film takes place, and (iii) *the outer region*, the uniform ultra-thin film that extends indefinitely away from the base of the droplet.

In region (iii), away from the droplet core, the ultra-thin film differs from the minimum thickness by exponentially small terms, $\bar{h}(x) \sim h_{\min}(\bar{p})$. To leading order, $h_{\min} \sim \epsilon$, solving (2.2) to next order as $\epsilon \to 0$ yields the dependence on the pressure,

$$h_{\min}(\bar{p}) \sim \epsilon + \epsilon^2 \frac{\bar{p}}{\mathcal{U}''(1)}. \tag{2.6}$$

Moreover, from (2.5) we also obtain that the droplet core satisfies $h_{\max}(\bar{p}) \sim -\mathcal{U}(1)/\bar{p}$. In the core region (i), the film thickness satisfies $\epsilon \ll \bar{h} \leq h_{\max}$, consequently the disjoining pressure is negligible, $\Pi(\bar{h}) = o(1)$. Therefore in the core, the leading order solution of (2.1) is a parabolic profile (see Figure 2),

$$\bar{h}(x) \sim \tfrac{1}{2}\bar{p}(\bar{w}^2 - x^2), \qquad \text{for } |x| \ll |\bar{w}|, \tag{2.7}$$

where the parameter $\bar{w}$ gives an effective measure of the width of the droplet. From (2.7), the maximum is given by $h_{\max} \sim \frac{1}{2}\bar{p}\bar{w}^2$. From this and the earlier estimate of $h_{\max}(\bar{p})$, we obtain the core width as

$$\bar{w}(\bar{p}) = \frac{A}{\bar{p}}, \qquad A \sim \sqrt{2|\mathcal{U}(1)|}. \tag{2.8}$$

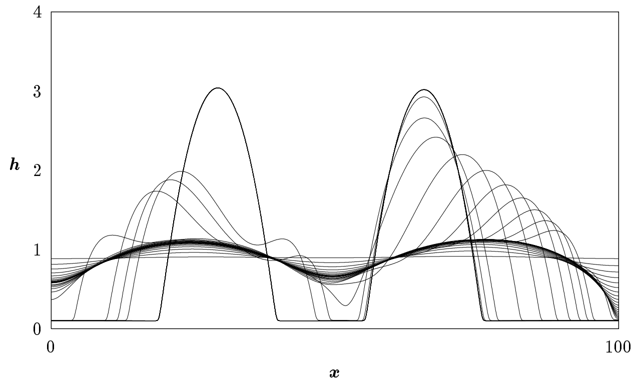

FIG. 4: The early stages of dewetting in thin films: instability of uniform fluid layer (with $h \approx 1$) leading to near-rupture of the film, the growth of holes in the layer (where $h \sim \epsilon$), and the coalescence of the fluid into isolated droplets.

Further interpretation of the constant A is provided by examining the contact line, region (ii). In this region, where the droplet core must asymptotically match to the ultra-thin film, we rescale the film thickness as $\bar{h}(x) = \epsilon \bar{H}(z)$, in a small neighborhood of the edge of the core, $x = -\bar{w} + \epsilon z$. Using these scalings, to leading order as $\epsilon \to 0$ (2.1) reduces to

$$\frac{d^2 \bar{H}}{dz^2} = \mathcal{U}'(\bar{H}), \tag{2.9}$$

and the local structure of the droplet contact line is given by the transition layer solution that satisfies $\bar{H}(z \to -\infty) \to 1$ and matches to the core region, $\bar{H}(z \to \infty) = O(\epsilon^{-1}) \to \infty$. Analogous to (2.3), the first integral of the leading order equation (2.9) is

$$\tfrac{1}{2}\left(\frac{d\bar{H}}{dz}\right)^2 = \mathcal{U}(\bar{H}) - \mathcal{U}(1), \tag{2.10}$$

Asymptotic matching of the slope of the solution for $z \to \infty$ then yields a measure of the macroscopic contact angle,

$$\left.\frac{d\bar{h}}{dx}\right|_{-\bar{w}} = \lim_{z\to\infty} \frac{d\bar{H}}{dz} = \sqrt{2|\mathcal{U}(\infty) - \mathcal{U}(1)|} = A, \tag{2.11}$$

The parameter A is a universal constant given in terms of the molecular potential $\mathcal{U}(\bar{H})$, and to leading order determines the contact angle independent of the ultra-thin film scale ϵ and the pressure $\bar{p}$. An important point is that (2.11) relates the interfacial energies to the contact angle, and is equivalent to the Young condition for shallow angles. This fact has been exploited in by other authors for the purpose of numerical computations [29, 43].

Finally, we define a mass of droplet as the mass of the core region,

$$\bar{m}(\bar{p}) \equiv \int_{-\bar{w}}^{\bar{w}} \bar{h}(x;\bar{p})\, dx \sim \frac{2A^3}{3\bar{p}^2}. \tag{2.12}$$

As a consequence, the size and mass of droplets may be measured in terms of the pressure $\bar{p}$. The error in this approximation of the mass is of the order of the thickness of the ultra-thin film and vanishes as $\epsilon \to 0$. We will make use of (2.12) later to relate conservation of mass to an evolution equation for the droplet pressure.

III. DYNAMICS OF THE ONE-DIMENSIONAL PROBLEM

Both analysis and numerical simulation identify a sequence of dynamical regimes for equation (1.10). Initially, a flat layer of fluid is subject to a long-wave instability (see figure 4). In the absence of conjoining effects in the pressure $\Pi(h)$, this instability would yield finite-time rupture of the fluid layer [42, 46]. For potentials of the form of $U(h)$, the fluid "dewets", it forms growing holes or "dry-spots" [10] where the layer narrows down to an ultra-thin film of height $h \sim \epsilon$. The fluid then rapidly converges to a series of parabolic-shaped droplets separated by the ultra thin film. Each droplet is very nearly an equilibrium solution like those already discussed. But there is a slow variation

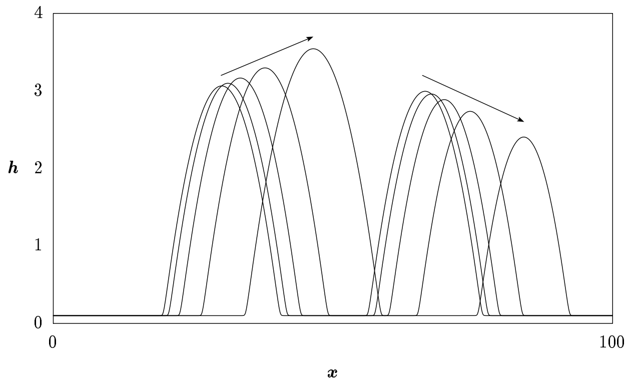

FIG. 5: Later stages in dewetting dynamics (continuing from Figure 4): once formed, the near-equilibrium fluid droplets evolve on a slower time-scale, with dynamics including both mass exchange and spatial drift.

in the outer mean field (the ultra-thin film) between neighboring droplets that leads to a coarsening process which governs the long-time evolution of the droplets.

Two features of the coarsening process are apparent (see figure 5). The first is that larger droplets gain mass at the expense of smaller droplets, in a fashion similar to Ostwald ripening. In our case, however, droplets also appear to move on timescales comparable to those of mass exchange. The causes for both of these phenomena will be explained next by a variational argument. A more systematic derivation of the dynamics follows.

A. Energy considerations

The slow process which ensues after the formation of metastable droplets may be understood by utilizing the mathematical structure of the evolution equation. Equation (1.10) has the energy

$$E(h) = \int U(h) + \tfrac{1}{2} h_x^2 \, dx, \tag{3.1}$$

which physically represents the combination of surface energy and intermolecular energies. Equation (1.10) in fact represents a generalized gradient flow (cf. [23]) of this energy and, subject to no-flux boundary conditions, the rate of energy dissipation is

$$\frac{dE}{dt} = -\int h^3 p_x^2 \, dx \leq 0. \tag{3.2}$$

There is an associated variational principle; the flux $J = -h^3 p_x$ minimizes the functional

$$F(J) = -\int \delta E J_x \, dx + \tfrac{1}{2} \int \frac{J^2}{h^3} \, dx, \tag{3.3}$$

where the first variation of the energy (3.1) is $\delta E = U'(h) - h_{xx} = p$. Evaluated at the minimizer, the first term in this functional is just the change in energy

$$-\int \delta E \, J_x \, dx = \int \delta E \, h_t \, dx = \frac{dE}{dt}. \tag{3.4}$$

Similarly, the second term in (3.3) is minus one half times the rate of energy dissipation.

To demonstrate that the coarsening process is energetically favorable, we show that the merger of two equal-sized droplets to form a single larger droplet and an UTF layer yields a decrease in energy. Within each droplet core, the film satisfies $h \gg \epsilon$, therefore the potential energy is negligible, and hence, using (2.8),

$$E(\text{two droplets}) \sim 2 \int_{-\bar{w}}^{\bar{w}} \tfrac{1}{2} h_x^2 \, dx \sim \frac{2A^3}{3\bar{p}}, \tag{3.5}$$

where the half-width of each droplet is $\bar{w} = A/\bar{p}$ (2.8). For comparison, in a single droplet with mass $2\bar{m}$, the corresponding pressure is $\tilde{p} \sim \bar{p}/\sqrt{2}$ and the half-width is $\tilde{w} \sim \sqrt{2}\,A/\bar{p}$. The merger of the two droplets creates an ultra-thin layer with the length $4\bar{w} - 2\tilde{w} \sim (4-2\sqrt{2})A/\bar{p}$. Hence the energy of the merged droplet is approximately

$$E(\text{single droplet and UTF}) \sim \frac{\sqrt{2}\,A^3}{3\bar{p}} + \frac{4-2\sqrt{2}}{\bar{p}} AU(\epsilon). \tag{3.6}$$

Not only is the surface energy of the droplet reduced relative to (3.5), but also the ultra-thin film further reduces the energy since the potential $U(\epsilon)$ is negative. Consequently, the total energy decreases as small droplets exchange mass through the UTF layer to form fewer, larger drops. This provides a driving force for the mass redistribution.

Since the energy is translation invariant, it may seem that there is no energetic advantage for droplets to move. Indeed, there is no energy lost in the translating process alone, and the first integral in (3.3) is essentially zero for a moving droplet. On the other hand, there will be non-zero fluxes in the ultra thin film on either side of the droplet. The flux minimizing the second term in (3.3) will therefore not be zero through the interior of the droplet, but rather is constrained to match the fluxes on either side of the droplet. As will be made precise in the following section, it is this flux which gives rise to droplet motion.

IV. DYNAMICS OF A SINGLE DROP

In the long-time dynamics of dewetting films, there is a slow evolution of droplets close to equilibrium. The droplets will move and change mass in response to fluxes imposed on them through the ultra thin film mean field. To explain this behavior, we first consider the evolution of a single droplet on a interval $-L \le x \le L$ that is large compared with the width of the droplet with fluxes (1.12) imposed at the boundaries,

$$J(-L) = \sigma \tilde{J}_-, \qquad J(L) = \sigma \tilde{J}_+, \tag{4.1}$$

where $\sigma > 0$ is a small parameter, together with the Neumann boundary conditions,

$$h_{xxx}(-L) = 0, \qquad h_{xxx}(L) = 0. \tag{4.2}$$

Note that in the no-flux case, $\tilde{J}_- = \tilde{J}_+ = 0$, these boundary conditions reduce to $h_x(\pm L) = h_{xxx}(\pm L) = 0$, the boundary value problem for equilibrium droplets on finite domains considered in [2]. As an initial condition, we will use the equilibrium droplet solution, centered at $x=0$, with initial pressure $\bar{p} = P_0$, $h(x,0) = \bar{h}(x;P_0)$. For any finite domain, $\bar{h}(x)$ is not an exact solution of the homogeneous boundary value problem, but it experiences only exponential small boundary influences and is called a quasi-equilibrium solution by Ward [40]. We will neglect these effects in the presence of finite fluxes.

Because droplets only change in response to the imposed flux, we introduce a new timescale selected by the scale of the fluxes,

$$\tau = \sigma t, \tag{4.3}$$

later we will relate σ to the other parameters in the model. Assuming that the solution evolves quasi-statically, we assume that the fluxes cause the position $X(\tau)$ and pressure $P(\tau)$ of the droplet to vary slowly in time and we seek a perturbation solution for $\sigma \to 0$ of the form

$$h(x,t) = \bar{h}(x - X(\tau); P(\tau)\,) + \sigma h_1(x,\tau) + O(\sigma^2). \tag{4.4}$$

Substituting this ansatz into the evolution equation (1.10) to leading order in σ yields

$$-\frac{\partial \bar{h}}{\partial x}\frac{dX}{d\tau} + \frac{\partial \bar{h}}{\partial \bar{p}}\frac{dP}{d\tau} = \mathcal{L}h_1, \tag{4.5}$$

where $\mathcal{L}$ is the linear operator for the spatial operator on the right side of (1.10),

$$\mathcal{L}g = \frac{\partial}{\partial x}\left(\bar{h}^3 \frac{\partial}{\partial x}\left[\Pi'(\bar{h})g - \frac{\partial^2 g}{\partial x^2}\right]\right), \tag{4.6}$$

subject to the boundary conditions given by (4.1, 4.2). Since the leading term in (4.4) represents a two-parameter, (X, P), family of homogeneous equilibrium solutions of (1.10) and $\mathcal{L}$ is a singular operator, the left side of (4.5) will need to satisfy two solvability conditions to ensure the existence of a unique solution for h_1. The solvability conditions, given by applications of the Fredholm alternative, are expressed in terms of orthogonality of the left side of (4.5) with the adjoint nullvectors, see Ward [40]. The operator $\mathcal{L}$ is not self-adjoint; the adjoint operator is

$$\mathcal{L}^\dagger \psi = \left(\Pi'(\bar{h}) - \frac{\partial^2}{\partial x^2} \right) \left[\frac{\partial}{\partial x} \left\{ \bar{h}^3 \frac{\partial \psi}{\partial x} \right\} \right]. \tag{4.7}$$

The null space of $\mathcal{L}^\dagger$ is two-dimensional and is spanned by the two bounded functions,

$$\psi_1(x) = 1, \qquad \psi_2(x) = \int_0^x \frac{\bar{h}(x') - h_{\min}}{\bar{h}(x')^3}\, dx'. \tag{4.8}$$

Taking the inner product of ψ_1 with (4.5) on $[-L, L]$ gives an equation for the evolution of the droplet pressure,

$$\frac{dP}{d\tau} = \left(\int_{-L}^{L} \frac{\partial \bar{h}}{\partial \bar{p}}\, dx \right)^{-1} (\tilde{J}_+ - \tilde{J}_-), \tag{4.9}$$

where we have used the fact that $\partial_x \bar{h}$ is an odd function with exponential decay outside of $[-\bar{w}, \bar{w}]$ to eliminate the contribution of the first term on the left in (4.5). Similarly, taking the inner product of ψ_2 with (4.5) using integration by parts, and again invoking even/odd symmetry gives an equation for the motion of the droplet,

$$\frac{dX}{d\tau} = - \left(\frac{\displaystyle\int_{-L}^{L} \frac{\bar{h} - h_{\min}}{\bar{h}^3}\, dx}{\displaystyle 2\int_{-L}^{L} \frac{(\bar{h} - h_{\min})^2}{\bar{h}^3}\, dx} \right) (\tilde{J}_+ + \tilde{J}_-). \tag{4.10}$$

At this point we note that σ is an artificial parameter, and we can eliminate it to write these two evolution equations in the original time-scale and in terms of the un-scaled fluxes as,

$$\frac{dP}{dt} = C_P(P, X)(J_+ - J_-), \qquad \frac{dX}{dt} = -C_X(P, X)(J_+ + J_-), \tag{4.11}$$

where C_P and C_X are coefficient functions given by the integrals of the equilibrium droplet $\bar{h}(x - X; P)$ in (4.9, 4.10).

We now examine the integrals in (4.9, 4.10) more closely to show that to leading order, these coefficients are only dependent on the droplet pressure P. In particular, we show that the dominant contributions to the coefficients are given by the droplet core and contact line regions, hence we reduce the integrals over the whole domain in (4.9, 4.10) to localized integrals over the droplet core. Consider C_X, since $\bar{h}(x)$ approaches $h_{\min}$ exponentially as $|x| \to \infty$, the integrands decay exponentially for $|x| \gg \bar{w}$, and we can either extend it to $(-\infty, \infty)$ or truncate the range of integration to $|x| \le \bar{w}$ with only small errors, so that

$$C_X \sim C_X(P) = \left(\frac{\displaystyle\int_{-\bar{w}}^{\bar{w}} \frac{\bar{h} - h_{\min}}{\bar{h}^3}\, dx}{\displaystyle 2\int_{-\bar{w}}^{\bar{w}} \frac{(\bar{h} - h_{\min})^2}{\bar{h}^3}\, dx} \right). \tag{4.12}$$

In practice, we evaluate this coefficient using integrals over $(-\infty, \infty)$ using the phase plane representation (2.3) of $\bar{h}(x)$, these integrals can be easily computed as singular integrals over $h_{\min} \le h \le h_{\max}$, the difference with exact evaluation of (4.12) is negligible. Note that since these integrals are translation invariant in x, C_X is independent of X.

A different approach must be applied to C_P since in the limit that $L \to \infty$, the integral in (4.10) diverges. This is because as $|x| \to \infty$, $\bar{h}(x) \to h_{\min}(\bar{p})$, and as in (2.6),

$$\frac{dh_{\min}}{d\bar{p}} = O(\epsilon^2), \tag{4.13}$$

so that the contribution to the integral from the ultra-thin film region will be $O(L\epsilon^2)$. As will be discussed further in the next section, we will restrict our attention to the regime where

$$\epsilon^2 L \ll 1. \tag{4.14}$$

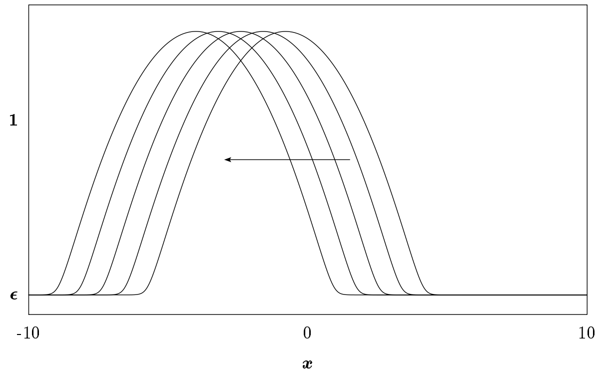

FIG. 6: Slow translational motion of a near-equilibrium droplet solution of (1.10) due to equal imposed fluxes (4.1).

Then the contribution from the ultra-thin film region will be negligible, and we can approximate the integral with one only over the droplet core:

$$C_P \sim C_P(P) = \left(\int_{-\bar{w}}^{\bar{w}} \frac{\partial \bar{h}}{\partial \bar{p}}\, dx \right)^{-1}, \tag{4.15}$$

to within $\mathcal{O}(\epsilon^2)$ errors. We calculate this coefficient from the definition of droplet mass (2.12), so that

$$C_P(P) = \left(\frac{d}{dp} \bar{m}(\bar{p}) \right)^{-1} \sim -\frac{4\bar{p}^3}{3A^3}. \tag{4.16}$$

Notice also that equation (4.9) is just a statement of conservation of mass in the form

$$\frac{dm}{dP}\frac{dP}{dt} = J_+ - J_-. \tag{4.17}$$

We conclude this section by illustrating the two special cases for the evolution laws (4.11) in which the two equations decouple:

- If $J_+ = J_-$, then $dP/dt = 0$, hence there is no change in pressure or mass of the droplet, this is a pure translation mode. In fact, since $C_X(P)$ is fixed, if the fluxes are held constant, then the solution is a constant velocity traveling pulse, $h \sim \bar{h}(x - ct; P)$, see Figure 6.
- If $J_+ = -J_-$, then $dX/dt = 0$, hence there is no change in the position of the droplet, this is a pure change-of-mass (pressure) mode, see Figure 7. For large drops (with small $\bar{p}$), the scaling relations found earlier suggest that this mode of evolution can be approximately described by a self-similar solution of the form $h(x,t) \sim \mathcal{H}(\,x/P(t)\,)/P(t)$.

In the next section we go on to study how the dynamics of a single droplet given by (4.11) can be used to describe the coupled dynamics of an array of interacting droplets.

V. DYNAMICS OF ARRAYS OF INTERACTING DROPLETS

We now make use of (4.11) as a building block to describe the dynamics for problems with multiple drops [9], the generic case of interest for dewetting films, where large numbers of droplets are typically initially formed.

Suppose now several droplets are present, connected to each other by an ultra-thin fluid layer with $h \sim \epsilon$. In this case, the fluxes imposed on each droplet are due to neighboring drops. Our goal is to derive asymptotically valid expressions for the fluxes $J_\pm$ (1.12) which then may be used to completely describe the evolution of droplets by using (4.11). This will involve a more careful examination of the structure of the ultra-thin film between the droplets.

Let L be a typical distance between droplets which is assumed large but no so large as to violate (4.14). In the UTF, rescale space using the new coordinate $z = \delta x$ where $\delta = L^{-1}$ is a small quantity. We also scale the film thickness by

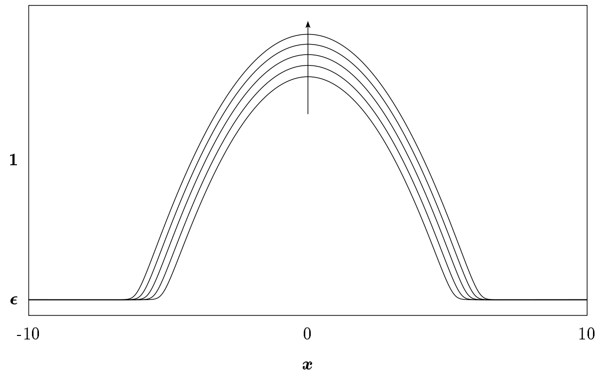

FIG. 7: Slow mass-growth of a near-equilibrium droplet solution of (1.10) due to opposite imposed fluxes (4.1).

$h = \epsilon H$. For droplets with fixed mass (and hence fixed pressure) the fluxes between drops will have the scale $O(\epsilon^3\delta)$, so the timescale is set by

$$\tau = \epsilon^3 \delta t. \tag{5.1}$$

In terms of the rescaled variables and (1.8), equation (1.10) yields the equation for the ultra-thin film,

$$\epsilon^2\delta^{-1}\frac{\partial H}{\partial \tau} = \frac{\partial}{\partial z}\left(H^3\frac{\partial}{\partial z}\left[\mathcal{U}'(H) - \epsilon^2\delta^2\frac{\partial^2 H}{\partial z^2}\right]\right). \tag{5.2}$$

First we note that for $\epsilon, \delta \to 0$, the last term in (5.2) is always negligible; this corresponds to the physical expectation that the curvature of the UTF is negligible compared to its disjoining pressure. Hence, to leading order (5.2) becomes the second-order nonlinear diffusion equation,

$$\epsilon^2\delta^{-1}\frac{\partial H}{\partial \tau} = \frac{\partial^2}{\partial z^2}\Big(\mathcal{V}(H)\Big), \tag{5.3}$$

where the "chemical potential" function $\mathcal{V}(H)$ is defined (up to an additive constant) by

$$\frac{d\mathcal{V}}{dH} = H^3\frac{d^2\mathcal{U}}{dH^2}. \tag{5.4}$$

In terms of the unscaled variables, we may define the corresponding quantity

$$\frac{dV}{dh} = h^3\frac{d^2U}{dh^2} \tag{5.5}$$

so that $V(h)$ is just a rescaling of $\mathcal{V}$:

$$V(h) = \epsilon^2\mathcal{V}(h/\epsilon). \tag{5.6}$$

Notice that the (unscaled) flux between droplets is therefore

$$J = -\partial_x V(h). \tag{5.7}$$

From (5.3) we note that if our assumption (4.14) on the thickness of the UTF compared to the separation length between droplets holds, then the ultra-thin film evolves quasi-statically, slaved to the evolution of the droplets. The structure of the ultra-thin film is then given by a solution of $\partial_{xx}V(h) = 0$ subject to the boundary conditions that $V(h)$ at a drop edge is $V(h_{\min})$ for that particular drop. Consequently, we obtain that the flux $-dV/dx$ between droplets is constant. In particular, the flux between two neighboring drops, labeled by k and $k+1$ and characterized by their positions X and pressures P, is given by

$$J_{k,k+1} = -\frac{V(h_{\min}(P_{k+1})) - V(h_{\min}(P_k))}{(X_{k+1} - \bar{w}(P_{k+1})) - (X_k + \bar{w}(P_k))}. \tag{5.8}$$

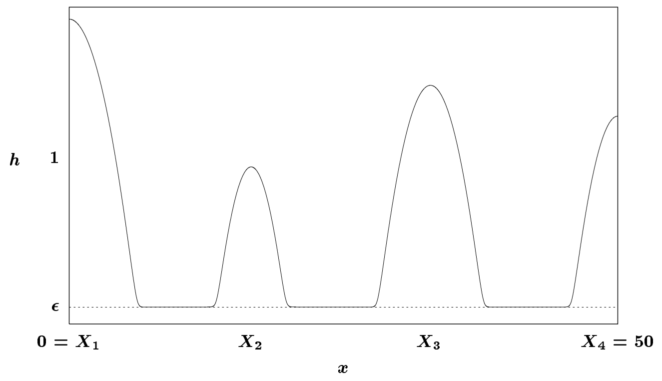

FIG. 8: The film thickness at time $t = 8000$ (after initial transients have vanished) from a numerical solution of (1.10) for $\epsilon = 0.1$ showing four well-defined drops with a connective ultra-thin film.

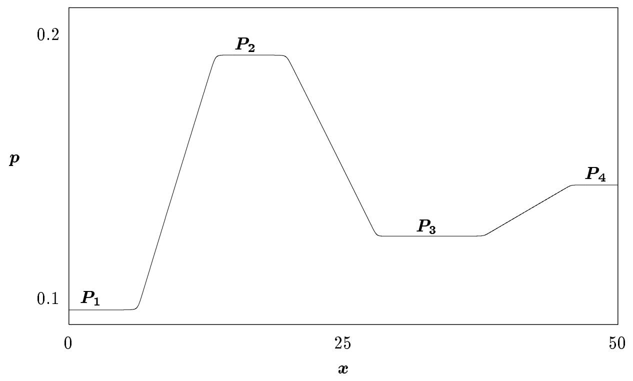

FIG. 9: The corresponding pressure (1.11) at $t = 8000$ for the solution shown in Figure 8. Note the near-constant pressure plateaus corresponding to the cores of the near-equilibrium droplets.

Since the thickness of the ultra thin film varies by only a small amount, the mobility coefficient in the definition of the flux (1.12) is always of the order $h^3 \sim \epsilon^3$. We conclude that since the flux is approximately constant, the pressure in the UTF is approximately piecewise linear. This is born out by the results of numerical simulations of (1.10), see Figures 8, 9.

In summary, we have reduced (1.10) to a system of $2N$ ordinary differential equations for the evolution of positions X_k and pressures P_k of an array of N drops,

$$\frac{dP_k}{dt} = C_P(P_k)(J_{k+1,k} - J_{k,k-1}), \qquad \frac{dX_k}{dt} = -C_X(P_k)(J_{k+1,k} + J_{k,k-1}), \qquad k = 1, 2, \cdots, N, \tag{5.9}$$

where the fluxes are defined by (5.8) and the coefficient functions are given by (4.12, 4.15).

These equations were integrated numerically using a fourth order Runge-Kutta scheme with an adaptive timestep. If a droplet shrinks in size, its mass decreases and hence by (2.12) its pressure increases. The pressure of the droplet will eventually become larger than $p_{\max}$, at which point the droplet is no longer near an equilibrium state. These "collapsing" droplets are very small and rapidly become part of the UTF mean field, so they are simply deleted from the array of finite drops when this occurs. Comparison of this coarsening model to the full PDE dynamics for a small array of drops is shown in Figures 10–11.

The second equation in (5.9) allows for motion of the droplets and hence the possibility of collisions between them. For practical computation of (5.9), we identify the onset of a collision when the contact lines of two neighboring droplets are within a $O(\epsilon)$ distance from each other. The dynamics of collisions are far from equilibrium, and hence occur on short time-scales compared to the near-equilibrium coarsening process. Neglecting the time of collision, the two drops are replaced by a single larger droplet with a pressure corresponding to the total mass of the two drops. The position of the resulting droplet was determined by the center of mass of the colliding droplets.

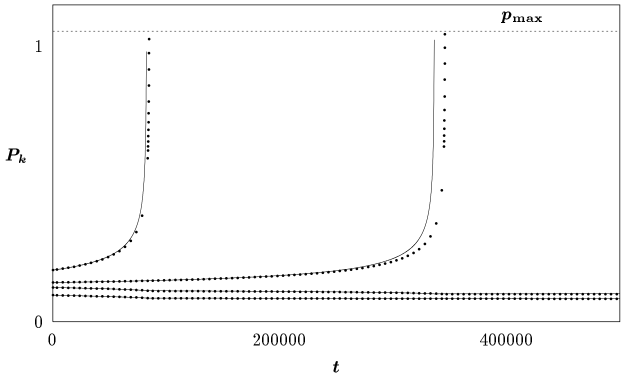

FIG. 10: Comparison of predictions for droplet pressures $P_k(t)$ from the direct numerical solution of the PDE (1.10) (dots) and the ODE model of coarsening (5.9) (solid curves) for the problem show in Figure 8. Note the collapse of two droplets as P_2 and P_4 exceed $p_{\max}$ in finite time.

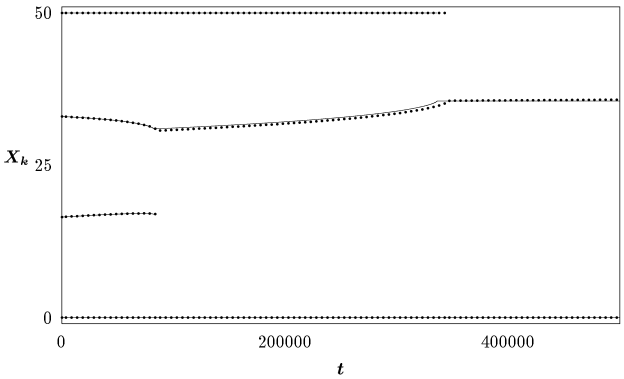

FIG. 11: Comparison of predictions for droplet positions $X_k(t)$ from the direct numerical solution of the PDE (1.10) (dots) and the ODE model of coarsening (5.9) (solid curves) for the problem show in Figure 8. The termination of the X_2 and X_4 branches occurs when those droplets collapse.

VI. SCALING LAW FOR THE DROPLET COARSENING PROCESS

Dewetting instabilities of nearly-uniform layers in large systems can be expected to form large numbers of droplets with comparable masses and similar separation distances [35, 36]. For long times, the array of droplets will evolve slowly according to the coarsening dynamics derived above. For such problems, the computational costs of direct simulations of the PDE (1.10) are prohibitive. Noting the timescales in Figures 10 and 11, the solution of (5.9) for large arrays for very long times can also become very costly. As an alternative to these numerical approaches, and to gain more insight into the physical mechanisms of the coarsening process in this problem, we derive a power-rule scaling law for the average number of drops at as a function of time, $N(t)$.

We now consider the coarsening dynamics for large arrays of drops, $N \to \infty$. As an example, we solve (5.9) starting from $N = 1000$ droplets of nearly equal mass, with large but nearly-uniform spacing between adjacent droplets, L, see Figure 12. Figure 13 shows the $X_k(t)$ world-lines for the positions of a typical subset of droplets in the array. In this example, there is relatively little drift of the droplets compared to their average spacing, so there were no collisions; the termination of $X_k(t)$ lines indicates collapse of those droplets. A log-log plot of the number of drops as a function of time for this simulation shows good agreement with a scaling law of the form

$$N(t) = O(t^{-2/5}), \tag{6.1}$$

see Figure 14. This behavior is reproduced for the long-time behavior from broad classes of initial data and appears to be the generic behavior of the coarsening process. We now present a heuristic argument for the occurrence of this power-law scaling behavior in the coarsening dynamics for dewetting.

This scaling behavior can be derived by considering the dynamics given by (5.9) that control the collapse of a single typical droplet in the array. Let this drop, with index k, have somewhat smaller mass (and hence higher pressure P_k)

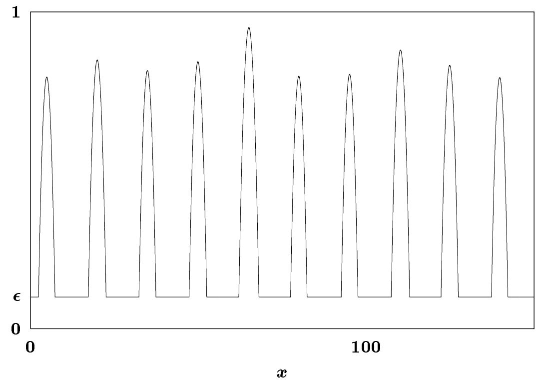

FIG. 12: Profiles of a typical subset of widely-spaced, nearly identical droplets considered in the analysis of the scaling properties of the coarsening process.

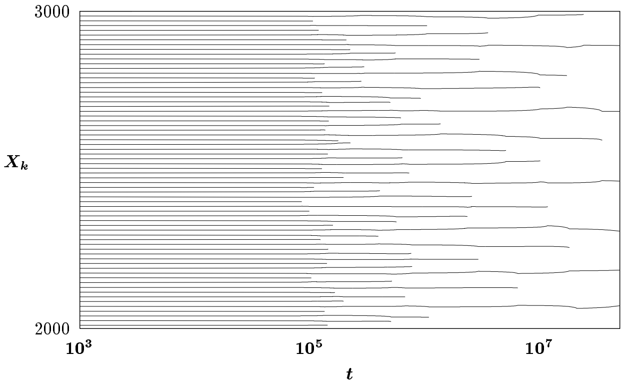

FIG. 13: World-lines $X_k(t)$ for a set of drops in a large array from a simulation of the coarsening dynamics given by (5.9). $X_k(t)$ lines end when a droplet collapses to negligible mass.

than its neighbors. We will assume that the separate between droplets, L is relatively large, so that we can neglect the droplet motion and focus on the equation for the evolution of the droplet pressures. By equation (4.16), we have $C_P \propto P^3$, and from (5.9) it is clear that droplets with larger pressures (that is smaller masses) evolve on faster time-scales. In fact, we will show that the collapse of small droplets occurs in finite-time. Using (2.6), to leading order the chemical potential yields $V(h_{\min}) \sim \epsilon^3 P$. Consequently, the flux (5.8) is approximated to leading order by

$$J_{k,k+1} \sim -\frac{\epsilon^3 P_{k+1} - \epsilon^3 P_k}{L}. \tag{6.2}$$

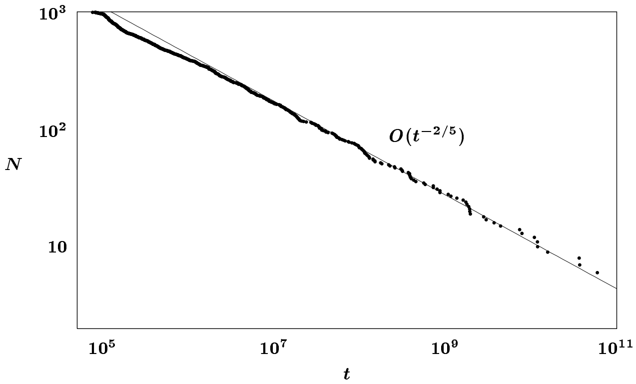

FIG. 14: Log-log plot of the number of drops as a function of time. A line corresponding to the scaling law (6.1) is shown for comparison.

Here we have assumed that $L \approx X_{k+1} - X_k$ is large compared to the average droplet width and that we can neglect the influence of droplet motion on the time-scale for pressure evolution. Therefore the pressure evolution equation becomes

$$\frac{dP_k}{dt} \propto \frac{\epsilon^3}{L} P_k^3 \left(P_{k+1} - 2P_k + P_{k-1}\right). \tag{6.3}$$

Since we have assumed that $P_k \gg P_{k\pm1}$, the time-scale for the evolution of P_k is much faster than that of its neighbors, therefore this equation further reduces to the local model,

$$\frac{dP_k}{dt} \propto -\frac{1}{L} P_k^4. \tag{6.4}$$

The solution of this model shows collapse of the droplet at in a finite-time, as the pressure diverges as $t \to T_c$,

$$P_k(t) \propto \left(\frac{T_c - t}{L}\right)^{-1/3}. \tag{6.5}$$

If the initial pressure of the collapsing drop is $\bar{P}_k$, then its collapse time scales like

$$T_c \propto \bar{P}_k^{-3} L \tag{6.6}$$

The typical droplet pressure relates to the mass by $M \propto \bar{P}^{-2}$ (see equation (2.12)). Both M and L scale like N^{-1} by the conservation of mass and the definition of the average separation distance on a finite size system, respectively. Therefore (6.6) yields the relation for the collapse timescale of the N^{th} droplet,

$$T_c \propto N^{-5/2}. \tag{6.7}$$

Note that during the collapse of each droplet, we assume that the separation distance L is approximately fixed. Although individual droplets will move, it seems evident again from the numerical simulations that the *average* droplet spacing will be unaffected. Therefore the scaling (6.7) should be correct when averaged over a large number of droplets. We also assume that L varies on a slower time-scale in response to reduction in the number of droplets due to collapse of individual drops, consistent with our assumption that the motion of droplets is slower than the evolution of pressures.

As can be seen from Figure 13, as time progresses, a roughly constant fraction of droplets vanish per unit time. We assume that the droplet collapses are independent uncorrelated events. Therefore, at a given time a constant fraction of droplets will be collapsing, which means that the droplet number $N(t)$ satisfies

$$\frac{dN}{dt} \propto -\frac{N}{T_c} \propto N^{-7/2}. \tag{6.8}$$

This may be integrated to yield the desired scaling relation,

$$N \propto t^{-2/5}. \tag{6.9}$$

VII. DISCUSSION AND CONCLUSIONS

We have given an asymptotic description of the late-stage coarsening dynamics of a one-dimensional dewetting thin film. A similar description is anticipated for two-dimensional films, where the inter-droplet flux will be derived from a two-dimensional elliptic boundary value problem analogous to (5.3). We also expect that a scaling law for the droplet number can be derived for two-dimensional films, which would be highly useful for comparison with experiments.

A further challenge would be to understand the asymptotics for small ϵ of droplets far from equilibrium. Since the addition of conjoining forces provides a regularization of the contact line motion, the limiting dynamics for small ϵ may provide insight into the connections between intermolecular forces and macroscopic models for contact line motion.

Our work has implications for coarsening processes in general. In certain regimes, it seems possible that collision of droplets, as opposed to their collapse, is the mechanism responsible for coarsening. Because the mathematical structure of our model is similar to those describing coarsening of binary mixtures, interface motion may be important for these processes as well.

Acknowledgments

We thank Andy Bernoff, Andrea Bertozzi and John Neu for useful suggestions. This research was supported by NSF FRG grant DMS-0074049. TPW was also supported by a fellowship from the Alfred P. Sloan foundation.

---

[1] J. Becker, G. Grun, R. Seemann, and K. Jacobs. Dynamical pattern formation upon dewetting. *LANL preprint cond-mat*, 0106313(1), 2001.

[2] A.L. Bertozzi, G. Grun, and T. P. Witelski. Dewetting films: bifurcations and concentrations. *Nonlinearity*, 14:1569–1592, 2001.

[3] J. Bischof, D. Scherer, S. Herminghaus, and P. Leiderer. Dewetting modes of thin metallic films: Nucleation of holes and spinodal dewetting. *Phys. Rev. Let.*, 77(8):1536–1539, 1996.

[4] J. P. Burelbach, S. G. Bankoff, and S. H. Davis. Nonlinear stability of evaporating/condensing liquid films. *J. Fluid Mech.*, 195:463–494, 1988.

[5] J. W. Cahn, C. M. Elliott, and A. Novick-Cohen. The Cahn-Hilliard equation with a concentration dependent mobility: motion by minus the Laplacian of the mean curvature. *European J. Appl. Math.*, 7(3):287–301, 1996.

[6] J. W. Cahn and J. E. Hilliard. Free energy of a nonuniform system I. Interfacial free energy. *J. Chem. Phys.*, 28:258–267, 1957.

[7] P. G. de Gennes. Wetting: Statics and dynamics. *Rev. Mod. Phys.*, 57:827, 1985.

[8] M. Elbaum, S. G. Lipsom, and J. F. Wettlaufer. Evaporation pre-empts complete wetting. *Europhys. Lett.*, 29(6):457–462, 1995.

[9] C. Elphick, E. Meron, and E. A. Spiegel. Patterns of propagating pulses. *SIAM J. Appl. Math.*, 50(2):490–503, 1990.

[10] A. Ghatak, R. Khanna, and A. Sharma. Dynamics and morphology of holes in dewetting thin films. *J. Coll. Int. Sci.*, 212:483–494, 1999.

[11] G. Grün and M. Rumpf. Nonnegativity preserving convergent schemes for the thin film equation. *Numer. Math.*, 87(1):113–152, 2000.

[12] S. Herminghaus, K. Jacobs, K. Mecke, J. Bischof, A. Fery, M. Ibn-Elhaj, and S. Schlagowski. Spinodal dewetting in liquid crystal and liquid metal films. *Science*, 282(5390):916–919, 1998.

[13] J. N. Israelachvili. *Intermolecular and surface forces.* Academic Press, New York, 1992. second edition.

[14] R. Konnur, K. Kargupta, and A. Sharma. Instability and morphology of thin liquid films on chemically heterogeneous substrates. *Phys. Rev. Let.*, 84(5):931–934, 2000.

[15] I. M. Lifshitz and V. V. Slyozov. The kinetics of precipitation from supersaturated solid solutions. *J. Chem. Phys. Solids*, 19:35–50, 1961.

[16] V. Mitlin. Dewetting revisited: new asymptotics of the film stability diagram and the metastable regime of nucleation and growth of dry zones. *J. Coll. Interface Sci.*, 227:371, 2000.

[17] V. Mitlin. Numerical study of a Lifshitz-Slyozov-like metastable dewetting model. *J. Coll. Interface Sci.*, 233:153–158, 2001.

[18] V. Mitlin and N. V. Petviashvilli. Nonlinear dynamics of dewetting: kinetically stable structures. *Phys. Lett. A*, 192:323, 1994.

[19] V. S. Mitlin. Dewetting of a solid surface: analogy with spinodal decomposition. *J. Coll. Int. Sci.*, 156:491–497, 1993.

[20] V. S. Mitlin and N. V. Petviashvili. Nonlinear dynamics of dewetting: kinetically stable structures. *Phys. Lett. A*, 192:323–326, 1994.

[21] A. Oron and S. G. Bankoff. Dewetting of a heated surface by an evaporating liquid film under conjoining/disjoing pressures. *J. Coll. Int. Sci.*, 218:152–166, 1999.

[22] A. Oron, S. H. Davis, and S. G. Bankoff. Long-scale evolution of thin liquid films. *Rev. Mod. Phys.*, 69(3):931–980, 1997.

[23] F. Otto. Dynamics of labrinthine pattern formation in magnetic fluids: A mean-field theory. *Arch. Rat. Mech. Anal.*, 141:63–103, 1998.

[24] R. L. Pego. Front migration in the nonlinear Cahn-Hilliard equation. *Proc. R. Soc. Lond. A*, 422:261–278, 1989.

[25] L. Pismen. Nonlocal diffuse interface theory of thin films and moving contact lines. *Phys. Rev. E.*, 64:021603, 2001.

[26] L. Pismen and Y. Pomeau. Nonlocal diffuse interface theory of thin films and the moving contact line. *Phys. Rev. E.*, 62:2840, 2000.

[27] G. Reiter. *Phys. Rev. Lett.*, 68:75–79, 1992.

[28] G. Reiter. Dewetting of thin polymer films. *Phys. Rev. Lett.*, 68(1):75–78, 1992.

[29] L. W. Schwarz, R. V. Roy, R. R. Eley, and S. Petrash. Dewetting patterns in a drying liquid film. *J. Colloid and Interface Sci.*, 234:363–374, 2001.

[30] R. Seemann, S. Herminghaus, and K. Jacobs. Dewetting patterns and molecular forces: a reconcilation. *Phys. Rev. Lett.*, 86(24):5534–5537, 2001.

[31] R. Seemann, S. Herminghaus, and K. Jacobs. Shape of a liquid front upon dewetting. *Phys. Rev. Lett.*, 87(19):196101, 2001.

[32] R. A. Segalman and P. F. Green. Dynamics of rims and the onset of spinodal dewetting at liquid/ liquid interfaces. *Macromolecules*, 32:801–807, 1999.

[33] A. Sharma and R. Khanna. Pattern formation in unstable thin liquid films. *Phys. Rev. Let.*, 81(16):3463–3466, 1998.
[34] A. Sharma and R. Khanna. Pattern formation in unstable thin liquid films under the influence of antagonistic short- and long-range forces. *J. Chem. Phys.*, 110(10):4929–4936, 1999.
[35] U. Thiele, M. G. Velarde, and K. Neuffer. Dewetting: film rupture by nucleation in the spinodal regime. *Phys. Rev. Lett.*, 87(1):016104, 2001.
[36] U. Thiele, M. G. Velarde, K. Neuffer, and Y. Pomeau. Film rupture in the diffuse interface model coupled to hydrodynamics. *Phys. Rev. E*, 64(3):031602, 2001.
[37] M. P. Valignat, S. Villette, J. Li, R. Barberi, R. Bartolino, E. Dubois-Violette, and A. M. Cazabat. Wetting and anchoring of a nematic liquid crystal on a rough surface. *Phys. Rev. Lett.*, 77(10):1994–1997, 1996.
[38] F. Vandenbrouck, M. P. Valignat, and A. M. Cazabat. Thin nematic films: metastability and spinodal dewetting. *Phys. Rev. Lett.*, 82(13):2693–2696, 1999.
[39] C. Wagner. Theorie for alterung von niederschlagen durch umlosen. *Z. Elektrochemie*, 65:581–594, 1961.
[40] M. J. Ward. Metastable dynamics and exponential asymptotics in multi-dimensional domains. In *Multiple-time-scale dynamical systems (Minneapolis, MN, 1997)*, pages 233–259. Springer, New York, 2001.
[41] M. B. Williams and S. H. Davis. Nonlinear theory of film rupture. *J. Coll. Int. Sci.*, 90:220–228, 1982.
[42] T. P. Witelski and A. J. Bernoff. Stability of self-similar solutions for van der Waals driven thin film rupture. *Phys. Fluids*, 11(9):2443–2445, 1999.
[43] H. S. Wong, S. Morris, and C.J. Radke. Three-dimensional menisci in polygonal capillaries. *J. Colloid and Interface Sci*, 148:317–336, 1992.
[44] R. Xie, A. Karim, J. F. Douglas, C. C. Han, and R. A. Weiss. Spinodal dewetting of thin polymer films. *Phys. Rev. Let.*, 81(6):1251–1254, 1998.
[45] B. D. Yang and O. C. K. Tsui. Critical thickness in dewetting films. *LANL preprint cond-mat*, 0110123(1), 2001.
[46] W. W. Zhang and J. R. Lister. Similarity solutions for van der Waals rupture of a thin film on a solid substrate. *Phys. Fluids*, 11(9):2454–2462, 1999.